Synoptic Weather Types for the Ross Sea Region, Antarctica

LANA COHEN

Antarctic Research Centre, Victoria University, Wellington, New Zealand

SAM DEAN AND JAMES RENWICK

National Institute of Water and Atmospheric Research, Wellington, New Zealand

(Manuscript received 24 November 2011, in final form 27 June 2012)

ABSTRACT

Synoptic classifications over the Southern Ocean in the Ross Sea region of Antarctica (50°S–Antarctic coast, 150°E–90°W) have been derived from NCEP reanalysis data (1979–2011), producing a set of six synoptic types for the region. These types describe realistic synoptic conditions for the region and represent the moisture-bearing low pressure systems that circulate around Antarctica. The types are described as follows: low Bellingshausen/Amundsen (L-BA), low (L), zonal (Z), low Ross (L-R), ridge (R), and low Amundsen (L-A).

Seasonal frequencies of the synoptic types reflect the seasonal zonal shift of the Amundsen Sea low (ASL) and also correlate well with the Southern Oscillation index (SOI) and the southern annular mode (SAM). Variability in the occurrences of the synoptic types L-R and L-BA indicate a shifting of the position of the ASL farther east (west) toward (away from) the Antarctic Peninsula during La Niña (El Niño) and positive (negative) SAM conditions. A joint linear regression of the SOI and SAM indices show the strongest correlations with the types L-BA and L-R in the spring and quantifies the joint forcing effect of these climate cycles on synoptic variability in the region.

As a demonstration of how synoptic classification provides links between large-scale atmospheric circulation and local climate parameters, the synoptic types are related to precipitation and temperature at Roosevelt Island, an ice core site on the Ross Ice Shelf (80°S, 160°W). The synoptic types provide quantification of distinct precipitation and temperature regimes at this site, which allows for more fundamental understanding of the precipitation source regions and transport pathways that drive the variability in snow and ice proxies.

1. Introduction

Understanding the links between large-scale atmospheric circulation and local meteorological parameters is the subject of many studies (e.g., Smithson 1986; Yarnal et al. 2001; Sheridan and Lee 2010). One technique for investigating these links is synoptic-climatological classification, which groups synoptic weather patterns into distinct regimes and relates them to local or regional climate parameters (Yarnal 1993). A synoptic-climatological classification (known locally as ''Kidson types'') was developed for New Zealand (Kidson 1994, 2000) that showed relationships between the synoptic regimes and climate parameters such as precipitation and temperature as well as relationships to large-scale atmospheric circulation patterns such as those induced by the El Niño–Southern Oscillation (ENSO) and the southern annular mode (SAM) (Kidson 1999; Kidson and Renwick 2002; Renwick 2011). Kidson's synoptic typing has been shown to have many uses both qualitatively and quantitatively, through analysis of paleoclimate proxies (Lorrey et al. 2007), biological systems (Renwick et al. 1998), and glacier mass balance (Purdie et al. 2011).

This study uses Kidson's synoptic classification techniques and applies it to the Ross Sea region of Antarctica. While much work has been done to understand both past and present Antarctic climate using snow and ice reconstructions, station data, satellite and reanalysis data, and climate models, less has been done on synoptic scales. Studies of Antarctic climate indicate that climate variability is not homogeneous over the entire continent (Turner et al. 2005a; Rignot et al. 2008; O'Donnell et al. 2011). Specific interest lies in the Pacific sector of

Corresponding author address: Lana Cohen, Antarctic Research Centre, Victoria University, P.O. Box 600, Wellington 6140, New Zealand.
E-mail: lana.cohen@vuw.ac.nz

DOI: 10.1175/JCLI-D-11-00690.1

Antarctica, the region encompassing the Ross Sea, West Antarctica, and the Antarctic Peninsula, because of these region's importance for understanding variability in ENSO and the SAM, the stability of the Ross Ice Shelf, mass balance of the West Antarctic Ice Sheet, and sea ice distribution (Mayewski et al. 2005; Fogt and Bromwich 2006; Krinner et al. 2007; Stammerjohn et al. 2008).

Climatologically, this region is dominated by the Amundsen Sea low (ASL), a permanent region of low pressure within the circumpolar trough that spans the Bellingshausen, Amundsen, and Ross Seas at ~65°–70°S. The ASL is of great interest as it has measurable effects on the climate of West Antarctica and the Amundsen, Bellingshausen, and Ross Sea regions. It is a region of significant cyclonicity and is known to be affected by large-scale atmospheric circulation variability (Bromwich 1988; Cullather et al. 1996; Simmonds et al. 2003; Fogt et al. 2012).

Synoptic-scale systems have been shown to be very important for determining the amount and distribution of precipitation in Antarctica (Noone et al. 1999; Noone and Simmonds 2002). As such, synoptic-climatological classification can provide further understanding of the synoptic controls on precipitation, which is important for interpreting snow and ice paleoclimate archives. As a case study, we investigate how the synoptic types relate to precipitation at Roosevelt Island, the site of a future ice core record, on the eastern side of the Ross Ice Shelf. While previous studies have used back trajectories to understand precipitation delivery for interpreting snow and ice records in Antarctica (e.g., Helsen et al. 2007; Thomas and Bracegirdle 2009; Sinclair et al. 2010), synoptic-climatological classification is a more general approach with the potential to relate precipitation (and other meteorological parameters) over a much larger region and also to provide a link to large-scale atmospheric circulation.

2. Data and methods

a. NCEP reanalysis: Geopotential height data

Reanalysis data have been widely used to analyze Antarctic climate variability, examine atmospheric circulation patterns, and correlate with snow and ice records (King and Turner 1997). This study uses the National Centers for Environmental Prediction–National Center for Atmospheric Research (NCEP–NCAR) reanalysis dataset, which assimilates and reprocesses in situ meteorological data and satellite data to produce a comprehensive global dataset of meteorological parameters at 2.5° latitude/longitude resolution (though the underlying models are run at higher resolution) (Kalnay et al. 1996). The NCEP–NCAR dataset extends from 1948 to the present, but parameters for the high latitudes are more reliable since the incorporation of satellite-based observations in 1979 (Bromwich and Fogt 2004; Bromwich et al. 2007). This study uses twice-daily (0000 and 1200 UTC) land-masked 1000-hPa geopotential heights for the time period 1 January 1979–30 June 2011.

b. Climate indices

Climate indices for the El Niño–Southern Oscillation and the southern annular mode are used in this study to investigate how the synoptic types relate to large-scale climate variability. The SAM is the expansion and contraction of the polar vortex and involves a mass shift in the atmosphere in the middle to high latitudes (Thompson and Wallace 2000). We use the SAM index from Marshall (2003), which is a proxy for the zonal-mean sea level pressure difference between 40° and 65°S and is derived from station data, as opposed to reanalysis data. Positive values of the SAM indicate lower surface pressure over Antarctica and higher pressures at midlatitudes.

The El Niño–Southern Oscillation describes a coupled oceanic–atmospheric climate cycle that is primarily expressed as anomalies in sea surface temperature, wind, and pressure in the tropical Pacific Ocean. The variability in ENSO can be measured by the Southern Oscillation index (SOI), which expresses the strength and phase of ENSO events, where a negative SOI is an El Niño (warm) event and a positive SOI is a La Niña (cold) event. The SOI is calculated from the difference in monthly-mean sea level pressure anomalies between Tahiti and Darwin (Trenberth 1997).

c. Cluster analysis

Cluster analysis was performed on NCEP reanalysis geopotential height data over the ocean and Ross Ice Shelf for the region encompassing the Ross and Amundsen Seas and part of the Bellingshausen Sea (50°S–Antarctic coast, 150°E–90°W) (Fig. 1). Slightly larger and smaller areas of analysis were also considered but did not affect the results materially. This region appeared to be the best to represent the synoptic conditions of the region as it is an area small enough to capture synoptic weather patterns but not so large as to have too many patterns to combine into meaningful clusters. The cluster analysis gives similar patterns for 500- and 1000-hPa geopotential heights, but we use the 1000-hPa fields for this study as they show more spatial variability in the pressure fields than the 500-hPa fields. Kidson (2000) showed in his analysis for the New Zealand region that the relationship between synoptic types and meteorological parameters

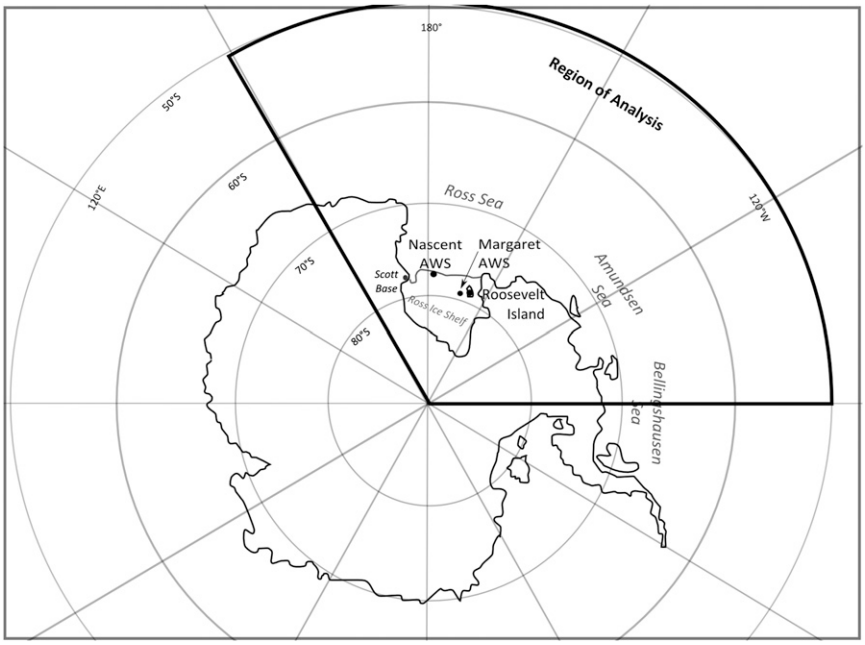

FIG. 1. Map indicating area of cluster analysis (50°S–Antarctic coast, 150°E–90°W). Locations of Roosevelt Island ice core site and Nascent and Margaret automatic weather stations (AMRC, SSEC, UW-Madison) are also indicated.

did not differ significantly between the 500- and 1000-hPa-derived types.

Prior to clustering, the data were detrended (mean subtracted), area weighted (by the cosine of the latitude), and land masked to remove the effects of continental topography. Cluster analysis was performed on the dataset of twice-daily geopotential height patterns (for all months of the year combined) based on the convergent *k*-means procedure (MacQueen 1967). The initial clusters are generated from a random selection of N ''seed'' patterns from the full set of synoptic fields. Each geopotential map state (23 738 time points) is then matched to one of the N initial clusters based on the minimum root-mean-square difference (*k* means) between the standardized means of each pattern. Every pattern is assigned to one of the initial N clusters. At each iteration, clusters are merged based on the two clusters with the highest pattern correlation and the patterns are then reassigned to the new clusters. Thus, the procedure goes from N clusters to $N - 1$ clusters, $N - 2$ clusters, and so on, eventually to one cluster containing all the data.

Since the final number of clusters chosen to represent a dataset can be arbitrary, determining this number was done by running the clustering procedure 10 times using 50 different randomly selected seed clusters. This provided an assessment of cluster reproducibility and stability. The final selection of the number of clusters to retain was made by visual inspection. The procedure produced a consistently reproducible set of six clusters for every run. The frequency of cluster occurrence is calculated for each set of clusters. For all 10 runs, the frequency of the six clusters varied by only 0.1%.

The clustering procedure was also run using the European Centre for Medium-Range Weather Forecasts (ECMWF) Interim Re-Analysis (ERA-Interim) dataset, which is now available from 1979 onward. The ERA-Interim 1000-hPa geopotential height fields for 1979–2011 produced identical clusters to the NCEP data with cluster frequency differing from the NCEP clusters by only 0.4%–0.8%.

d. Assessment of NCEP reanalysis precipitation data

Because there are no in situ precipitation measurements for our case-study site, Roosevelt Island (80°S, 160°W, 550 m MSL), we will be using precipitation rates from the NCEP reanalysis dataset in conjunction with the synoptic types. Previous assessments of NCEP reanalysis precipitation over Antarctica urge using this data with caution (e.g., Bromwich et al. 2007; Bromwich et al. 2011). We compare a 2-yr in situ precipitation record from the Ross Ice Shelf to NCEP reanalysis precipitation fluxes for the nearest grid box to qualitatively assess how well the reanalysis data represent precipitation on the Ross Ice Shelf.

The recent analysis from Bromwich et al. (2011) indicates that, for the NCEP dataset, the net accumulation

($P - E$) over Antarctica does not compare well to several other reanalysis products, though they show that the discrepancies lay primarily with the evaporation term and the precipitation actually compares well to the other reanalyses products. The best agreements regionally are for the Ross Ice Shelf and parts of West Antarctica though the precipitation does show a spurious upward trend (since 1979) in the Pacific sector that is not seen in the other reanalyses. The source of this trend is unknown but may be related to the strong negative trend in pressure also seen in this region (Bromwich et al. 2011).

The University of Wisconsin—Madison (UW-Madison) Antarctic Meteorological Research Center (AMRC) automatic weather station (AWS) ''Nascent'' (78°S, 178.5°W) is located near the northwestern edge of the Ross Ice Shelf, approximately 340 km west of Roosevelt Island (Fig. 1). Snow surface height and other meteorological parameters were measured by the Nascent AWS for the period 1 January 2009–30 April 2011. Snow accumulation (and ablation) was measured with a Campbell Scientific SR50 acoustic depth gauge (ADG), which measures the distance to the snow surface using reflected sonic pulses. Detailed specifications on all of the AWS instrumentation can be found on the University of Wisconsin AMRC website (http://amrc.ssec.wisc.edu). The Nascent station raw data were retrieved from the University of Wisconsin AMRC ftp site (ftp://amrc.ssec.wisc.edu).

A snow accumulation record for the Nascent station was produced from the raw data by first removing null measurements and measurements obviously affected by rime, wind, and blowing snow (i.e., spurious data points outside of the 2-yr range of values). The raw snow-height data were recorded at 20-min intervals and were averaged to the same 6-hourly resolution as the reanalysis data (18-point average). The NCEP reanalysis data are given as an instantaneous precipitation rate: kg m^{-2} s^{-1} water equivalent (w.e.). To compare with the snow accumulation that is measured by the ADG, the reanalysis data were converted to mm w.e. $(6\ h)^{-1}$ and summed.

e. Surface temperature data

The relationship between surface temperature at Roosevelt Island and synoptic types is investigated using air temperature data from a University of Wisconsin AWS located less than 100 km west of Roosevelt Island (''Margaret'': 80°S, 165°W, 67 m MSL) and NCEP reanalysis surface temperature for the grid box at 80°S, 160°W. The NCEP reanalysis temperature data are twice daily for the period 1 January 1979–30 June 2011. The Margaret AWS dataset is 3-hourly for the period 13 November 2008–30 June 2011.

The Margaret AWS data were retrieved from the University of Wisconsin AMRC Space Science and Engineering (SSEC) ftp site (ftp://amrc.ssec.wisc.edu). Air temperature is measured with a platinum resistance thermometer sensor with accuracy of ±0.5°C (further specifications on the University of Wisconsin AWS instrumentation is at http://amrc.ssec.wisc.edu). The AWS 3-hourly data have been preprocessed to remove erroneous data and were then averaged to 12 h to match the resolution of the synoptic typing. Monthly means were calculated for the respective datasets and subtracted from each data point before grouping by synoptic type.

3. Results

a. Synoptic types

Figure 2 shows the six synoptic types for the Ross Sea region resulting from the 1000-hPa geopotential height cluster analysis. These six types are a classification of all synoptic conditions for the period 1979–2011. The patterns have larger spatial extents than typical synoptic pressure systems because of the smoothing that results from averaging many patterns together, but they show realistic synoptic conditions for the region that is dominated by cyclonic, moisture-bearing low pressure systems that travel around the continent with the westerly circumpolar winds. Note that the process of clustering inherently emphasizes the differences in strength and positions between the patterns.

The types are described as follows: low Bellingshausen/Amundsen (L-BA), low (L), zonal (Z), low Ross (L-R), ridge (R), and low Amundsen (L-A). All of the patterns but zonal are characterized by low pressure systems with centers of action about 60°S located in different parts of the Ross, Amundsen, and Bellingshausen Seas. The zonal pattern is characterized by a relatively weak latitudinal pressure gradient. The patterns are, in order of frequency, noted on each map, with the type L-BA as the most frequent pattern (30.8%) and the remaining five patterns occurring significantly less but about equally (12%–15.3%). Generally, the synoptic patterns are less diverse than those derived for midlatitude regions such as New Zealand, which reflects the dominance of low pressure systems in the atmospheric circulation around Antarctica.

b. Seasonal variation of synoptic types

The seasonal variability of the Ross Sea region synoptic types is shown in Fig. 3. The most obvious seasonal change reflects the well-known zonal shift of the Amundsen Sea low, the region of permanent low pressure that spans the Bellingshausen, Amundsen, and Ross Seas at ~65°–70°S (King and Turner 1997; Simmonds

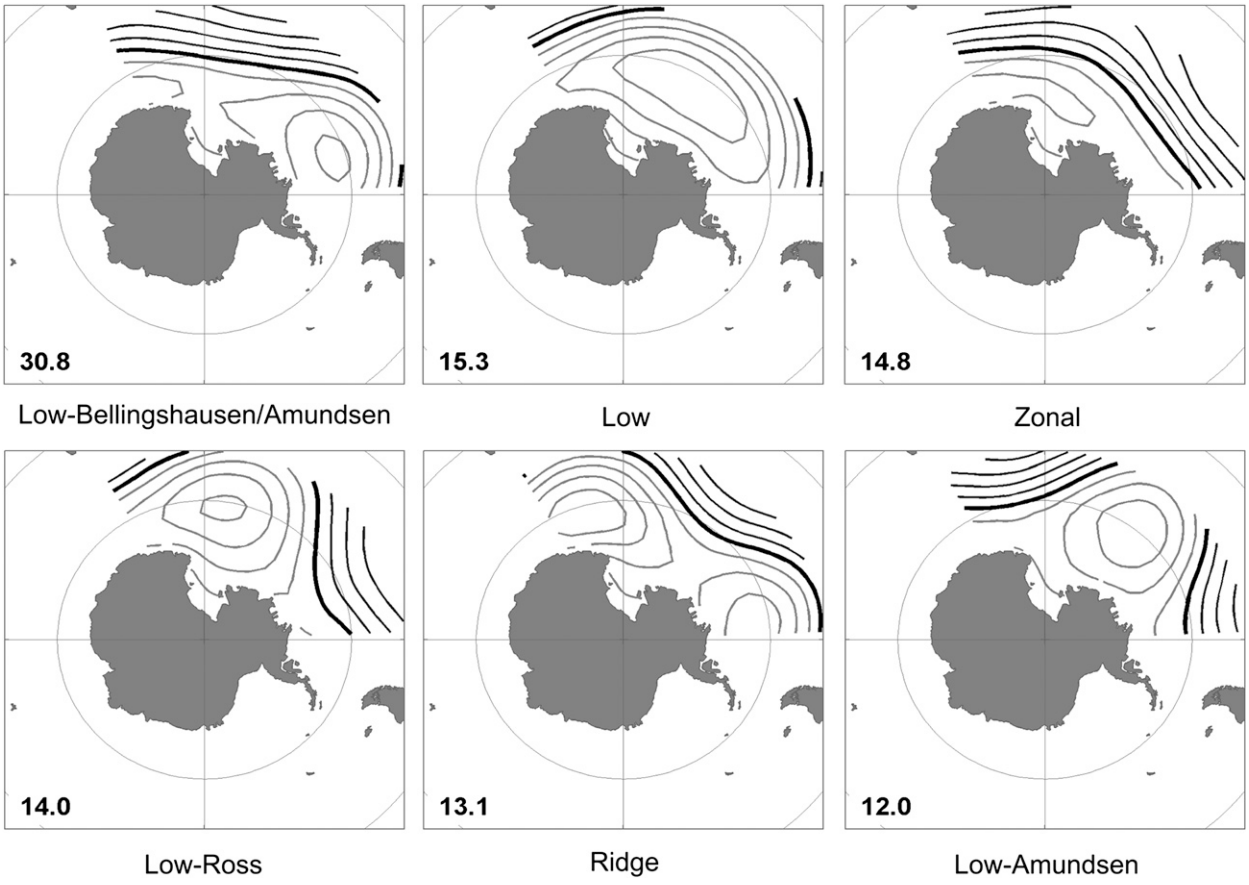

FIG. 2. Synoptic types for Ross Sea region from NCEP reanalysis 1000-hPa geopotential height data from 1 Jan 1979 to 30 Jun 2011. The thick black lines are zero meters, the light gray lines are negative, and the dark gray lines are positive. The contour interval is 20 m. The northern limit of the plots is 50°S; the inner circle is 60°S. Frequency of occurrence is shown in bottom-left corner of each type.

et al. 2003; Fogt et al. 2012). The occurrence of the type L-BA is more frequent in summer [December–February (DJF)] and autumn [March–May (MAM)] while the type L-R is more frequent in spring [September–November (SON)] and winter [June–August (JJA)], indicating that the region of low pressure shifts farther east (west) toward the Bellingshausen Sea (Ross Sea) in the summer and autumn (winter and spring).

During the spring, the type L has significantly increased occurrence, while the type L-A is decreased in occurrence. Both of the types L and L-A are lows centered at ~60°S, 135°W, with type L being much broader and deeper than L-A. The seasonal shift between these two types may be a reflection of the semiannual oscillation (SAO). The SAO is the climatological expansion and contraction of the circumpolar trough during the equinoctial months when temperature and pressure gradients are largest between middle and high latitudes. These gradients result in higher baroclinicity and stronger westerlies in the region south of ~50°S, which give rise to deeper and more southerly (and easterly) pressure systems during the spring and autumn with strongest maxima seen in spring (van Loon 1967; van den Broeke 1998; Simmonds and Jones 1998). The SAO has significant influence on sea ice and meteorological parameters for many regions of Antarctica (Simmonds and Jones 1998; van den Broeke 1998; 2000), but it exhibits its largest variability in pressure in the Amundsen Sea region and demonstrates this variability on interannual to decadal time scales (Simmonds and Jones 1998; Simmonds 2003).

c. Relation to circulation indices SOI and SAM

Two dominant modes of atmospheric variability that are known to have significant influences on southern high latitudes are the ENSO and the SAM. ENSO influences the high-latitude circulation on interannual and longer time scales while the SAM plays a significant role on all time scales from the synoptic to interannual or

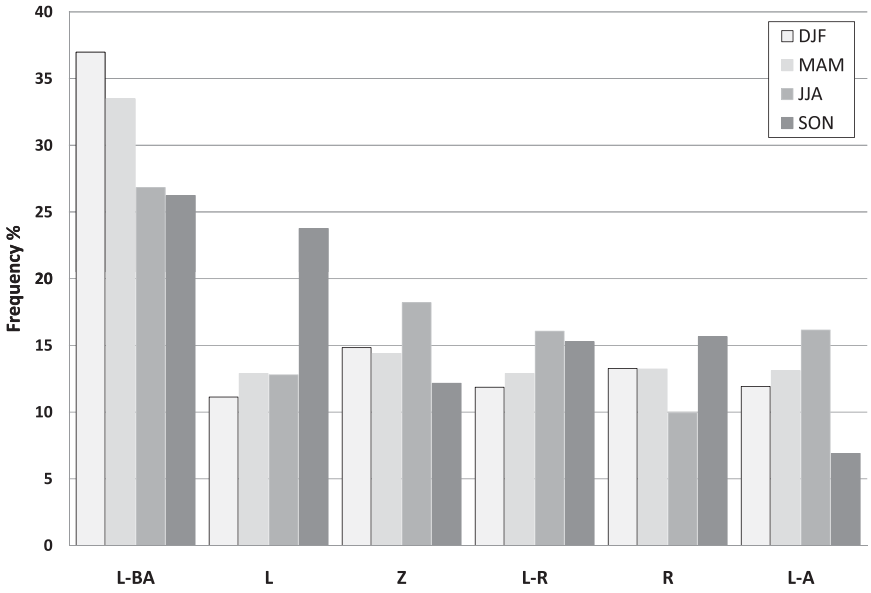

FIG. 3. Seasonal variability of synoptic types by frequency of occurrence from 1979 to 2011. The synoptic types correspond to those in Fig. 2: low Bellingshausen/Amundsen, low, zonal, low Ross, ridge, and low Amundsen.

longer (Thompson and Wallace 2000; Turner 2004). In Antarctica, evidence of these climatic patterns has been found to be strongest in the Ross and Amundsen Sea regions, but the interactions between them are complex and still not well understood and there is no real consensus of how these cycles are manifest in the region (e.g., Bromwich et al. 2000; Renwick 2002; Schneider et al. 2004; L'Heureux and Thompson 2006; Fogt and Bromwich 2006; Gregory and Noone 2008).

Table 1 shows seasonal correlations r and significance levels p of seasonal-mean synoptic type occurrence frequency with indices for the SAM (Marshall 2003) and the SOI [from the National Oceanic and Atmospheric Administration/Climate Prediction Center (NOAA/CPC)]. The indices and synoptic type frequencies are averaged seasonally from monthly values. The strongest correlations with synoptic types are with the SAM in all seasons with the exception of a strong negative correlation of the type L-R with the SOI in the spring. The types L-BA and L-R show the strongest correlations with both the SOI and the SAM, with L-BA being positively correlated and L-R being negatively correlated. The positive (negative) correlation of L-BA (L-R) with the SAM is in line with previous studies showing the shifting of the position of the Amundsen Sea low farther east (west) toward (away from) the Antarctic Peninsula during positive (negative) SAM conditions (e.g., Kwok and Comiso 2002; Turner et al. 2005b). The correlations of the types L-BA and L-R with the SOI indicate there is similar variability in the ASL with ENSO. Positive correlations of the SOI with L-BA show La Niña conditions shift the position farther east toward Bellingshausen Sea while negative correlations of the SOI with L-R show El Niño conditions shift the position farther west toward the Ross Sea.

TABLE 1. Seasonal correlations r and significance levels p for synoptic type occurrence with the SOI and the SAM over the period 1979–2011. Boldface values indicate correlations with 95% significance levels ($p < 0.05$).

	DJF				MAM				JJA				SON			
	SOI		SAM		SOI		SAM		SOI		SAM		SOI		SAM	
	R	*p*	*r*	*p*	*r*	*P*	*r*	*p*	*r*	*P*	*r*	*p*	*r*	*p*	*r*	*p*
L-BA	0.259	0.152	−0.013	0.945	**0.427**	**0.013**	**0.565**	**0.001**	**0.402**	**0.023**	**0.352**	**0.048**	0.291	0.106	**0.753**	**0.000**
L	**0.439**	**0.012**	**0.439**	**0.012**	−0.055	0.761	−0.099	0.585	0.189	0.300	**0.476**	**0.006**	0.329	0.066	−0.024	0.897
Z	−0.331	0.065	−0.076	0.678	−0.306	0.084	−0.067	0.710	−0.052	0.778	−0.167	0.360	**−0.371**	**0.037**	−0.303	0.092
L-R	**−0.474**	**0.006**	−0.186	0.307	**−0.457**	**0.007**	**−0.491**	**0.004**	−0.248	0.171	**−0.552**	**0.001**	**−0.611**	**0.000**	**−0.547**	**0.001**
R	0.155	0.397	−0.121	0.509	0.262	0.141	0.184	0.305	**−0.464**	**0.007**	0.270	0.135	−0.016	0.932	−0.273	0.131
L-A	−0.057	0.758	−0.065	0.725	−0.077	0.668	**−0.482**	**0.005**	−0.117	0.522	**−0.421**	**0.016**	0.117	0.525	−0.179	0.327

TABLE 2. Seasonal correlations r and significance levels p for synoptic type occurrence with the upper and lower quartiles of the SOI and the SAM over the period 1979–2011. Boldface values indicate correlations with 95% significance levels ($p < 0.05$).

	DJF				MAM				JJA				SON			
	SOI		SAM		SOI		SAM		SOI		SAM		SOI		SAM	
	r	P	r	p	r	P	r	p	r	p	r	p	r	p	r	p
L-BA	0.416	0.109	0.020	0.941	**0.568**	**0.022**	**0.671**	**0.004**	**0.611**	**0.012**	0.428	0.098	0.316	0.234	**0.844**	**0.000**
L	**0.606**	**0.013**	0.460	0.073	−0.087	0.748	−0.059	0.828	0.280	0.294	**0.549**	**0.027**	0.457	0.075	−0.049	0.856
Z	−0.394	0.131	−0.047	0.863	−0.362	0.168	−0.117	0.667	−0.103	0.704	−0.216	0.422	−0.411	0.114	**−0.560**	**0.024**
L-R	**−0.549**	**0.028**	−0.219	0.416	**−0.612**	**0.012**	**−0.515**	**0.041**	−0.358	0.173	**−0.635**	**0.008**	**−0.697**	**0.003**	**−0.680**	**0.004**
R	0.166	0.539	−0.009	0.974	0.383	0.143	0.028	0.917	**−0.507**	**0.045**	0.340	0.198	−0.101	0.709	−0.239	0.373
L-A	−0.203	0.451	−0.222	0.409	−0.062	0.819	**−0.509**	**0.044**	−0.212	0.431	**−0.497**	**0.050**	0.166	0.538	−0.232	0.388

Table 2 shows the same seasonal correlations, but uses only the upper and lower quartiles for the SOI and the SAM ($-1 \geq$ SOI ≥ 1.2; $-0.79 \geq$ SAM ≥ 1.43), which reduces the number of values to 16 (significance levels >95% are bolded). The magnitudes of all the significant correlations in Table 1 are increased in Table 2, although a few are no longer significant because of the reduction in degrees of freedom. The SAM is strongly negatively correlated with the type L-R (strongest in the spring, $r = -0.68$) and strongly positively correlated with the type L-BA (also strongest in the spring, $r = 0.84$). The correlations in Tables 1 and 2 also show the type L occurs more frequently for +SAM and +SOI while the type L-A occurs more frequently for −SAM and −SOI. This is consistent with results from other studies (e.g., Fogt and Bromwich 2006; Fogt et al. 2011), which indicate a weaker (stronger) ASL during −SAM/El Niño (+SAM/La Niña) conditions.

To quantify the relative influences of ENSO and the SAM on the occurrence of these patterns, a multiple linear regression was calculated for both L-BA and L-R where

$$F_{\text{L-BA}} = a + b_{\text{SOI}}(\text{SOI}) + c_{\text{SAM}}(\text{SAM}).$$

The regressions were calculated using seasonally averaged values. Correlations and significance values are shown in Table 3. The multiple regressions improve on the correlations over either the SAM or SOI alone for all seasons except for summer and support results of previous studies concerning the linear (or near-linear) reinforcing of ''in phase'' events (i.e., +SAM/La Niña and −SAM/El Niño) on the climate of this region (e.g., Fogt and Bromwich 2006; Stammerjohn et al. 2008; Fogt et al. 2011; Markle et al. 2012). Correlations are highest for both L-BA and L-R in the spring ($r = 0.76$ and $r = 0.73$, respectively), indicating that the SAM and SOI jointly explain over 50% of the variance in frequency of these two types for this season.

The relative influences of normalized SOI and SAM indices on the multiple linear regressions are shown in Table 4, which gives the ratios of the coefficients, b_{SOI} and c_{SAM} (ratio of unity indicates equal strength of the predictors). For the spring, when there is the highest correlations with the regression, the SAM dominates the variance for L-BA ($b_{\text{SOI}}/c_{\text{SAM}} = 0.17$), while they are more equal for L-R ($b_{\text{SOI}}/c_{\text{SAM}} = 1.34$). The dominance of the SOI on L-R in summer is primarily due the influence of the very strong 1982/83 ENSO event (strongest during November–March).

We also investigate whether the trends seen in the SAM and SOI are reflected in the frequency of the synoptic types. Linear trends and significance values are calculated by season for the indices and synoptic type occurrence over the period 1979–2011 as shown in Table 5. The positive trends seen in the SOI (significance level >90%) for spring and summer are also seen in the type L for these months. The trends in type L may reflect an increase in the occurrence of the deeper, larger type L at the expense of the smaller, weaker type L-A (negative trend in L-A significant at >95% level for MAM). This scenario would be consistent with previous investigations of cyclone activity in the Southern Hemisphere, which show increasing size and depth (and decreasing number) of cyclonic systems in this region with positive SOI and positive SAM (e.g., Simmonds and Keay 2000; Simmonds et al. 2003; Pezza et al. 2012). Interestingly, the strongest (and most significant) trend is in type L (3.436 decade^{-1}, $p = 0.01$) during the spring instead of summer when both the SAM and SOI have significant positive trends. We would expect a stronger trend in the summer because of

TABLE 3. Correlations r and significance levels p for multiple linear regressions of SOI and SAM with types L-BA and L-R by season. Boldface values indicate correlations with 95% significance levels ($p < 0.05$).

	DJF		MAM		JJA		SON	
	r	p	r	p	r	p	r	p
L-BA	0.288	0.110	**0.639**	**0.000**	**0.552**	**0.001**	**0.761**	**0.000**
L-R	**0.474**	**0.006**	**0.603**	**0.000**	**0.621**	**0.000**	**0.733**	**0.000**

TABLE 4. Coefficients of the SOI and SAM regression with the types L-BA and L-R. Ratios of unity indicate equal influence on regression.

	DJF			MAM			JJA			SON		
	b_{SOI}	c_{SAM}	b_{SOI}/c_{SAM}	b_{SOI}	c_{SAM}	b_{SOI}/c_{SAM}	b_{SOI}	c_{SAM}	b_{SOI}/c_{SAM}	b_{SOI}	c_{SAM}	b_{SOI}/c_{SAM}
L-BA	1.37	−0.77	−1.78	3.01	4.34	0.69	3.67	2.56	1.43	0.82	4.96	0.17
L-R	−1.54	−0.001	1540	−2.20	−2.24	0.98	−2.11	−3.32	0.64	−2.51	−1.87	1.34

the reinforcing effects of a positive SOI and SAM on cyclonicity (Pezza et al. 2012). Thus, the strength of the trend in type L may be more of a reflection of the positive trend in the SAO since the early 1980s when it was very weak (van den Broeke 2000; Simmonds 2003).

d. Assessment of NCEP reanalysis precipitation data

Figure 4 shows snow accumulation for the Nascent AWS and precipitation accumulation for the NCEP reanalysis grid point 77.139°S, 178.125°W (T62 Gaussian grid) for the period 1 January 2009–30 April 2011. Since the AWS accumulation data are affected by densification, wind scour, and drifting (Knuth et al. 2010), objective identification of small and medium precipitation events is difficult. Large events can be easily identified in a subjective manner and these are shown in Fig. 4 by the smoothed line overlaying the AWS data. This line highlights the stepped jumps in surface height that indicate large precipitation events. Of the 13 large events seen in the AWS data, 9 are seen concurrently in the reanalysis data (~70%) and there are 6 large events in the reanalysis data that are not seen in the observed data (3 of these are in March–April 2011).

Total accumulation over the period is 0.835 m of snow for Nascent and 71.1 mm w.e. for the NCEP reanalysis. Using an average snow density of ~30% (Mellor 1964), the reanalysis data underestimate snow accumulation over this time period by a factor of ~3 (0.24-m total snow accumulation). While there are some previous studies showing that NCEP reanalysis tends to underestimate precipitation for many regions of Antarctica (e.g., Cullather et al. 1998; Zou et al. 2004), we are not aware of any which compare AWS observations and this discrepancy would be worth further investigation. Even though the magnitudes of reanalysis precipitation do not compare well to observed values, we feel the reanalysis data reproduce large precipitation events well enough to use the data in a qualitative sense to investigate how precipitation relates to the synoptic types.

e. Expression of synoptic types in precipitation

The relationship between precipitation at Roosevelt Island and the synoptic types is shown in Fig. 5. NCEP reanalysis twice-daily precipitation rates for Roosevelt Island are grouped by synoptic type for the same time period as the cluster analysis was run (1 January 1979–30 June 2011). The precipitation rates from NCEP reanalysis dataset are shown for each synoptic type by percentage of total accumulation and by distribution of sizes of precipitation events. The values of precipitation from the reanalysis data are only used in a relative sense as they are likely significantly underestimated for the Roosevelt Island site as discussed above.

The type L-R brings 29% of the total precipitation to the Roosevelt Island site even though it only occurs 14% of the time while the type L-BA, which occurs 30.8% of the time, brings only 19% of the precipitation to the site. The type L brings the least amount of precipitation (8%). As expected, the types L-R and L-A bring significant amounts of precipitation to the Roosevelt Island site, because these patterns deliver relatively warm moisture-bearing air from the Southern Ocean to the Antarctic

TABLE 5. Linear trends and significances for the SAM, SOI, and synoptic type frequencies calculated over the period 1979–June 2011 for each season. Boldface values indicate 95% significance levels ($p < 0.05$); italicized values indicate 90% significance levels ($p < 0.10$).

	DJF		MAM		JJA		SON	
	Linear trend (decade^{-1})	p	Linear trend (decade^{-1})	p	Linear trend (decade^{-1})	p	Linear trend (decade^{-1})	p
SOI	*0.677*	*0.07*	0.351	0.11	0.087	0.69	*0.465*	*0.08*
SAM	**0.468**	**0.04**	0.295	0.13	0.063	0.78	0.118	0.63
L-BA	−0.171	0.88	1.734	0.25	0.121	0.93	−0.980	0.50
L	*1.417*	*0.08*	0.231	0.82	0.906	0.36	**3.436**	**0.01**
Z	−0.538	0.57	−0.987	0.27	−0.050	0.96	−0.798	0.36
L-R	−0.580	0.51	−0.886	0.35	−1.361	0.22	−1.122	0.23
R	0.062	0.92	**1.350**	**0.04**	0.585	0.35	−0.576	0.43
L-A	−0.219	0.71	**−1.442**	**0.04**	−0.201	0.77	0.039	0.92

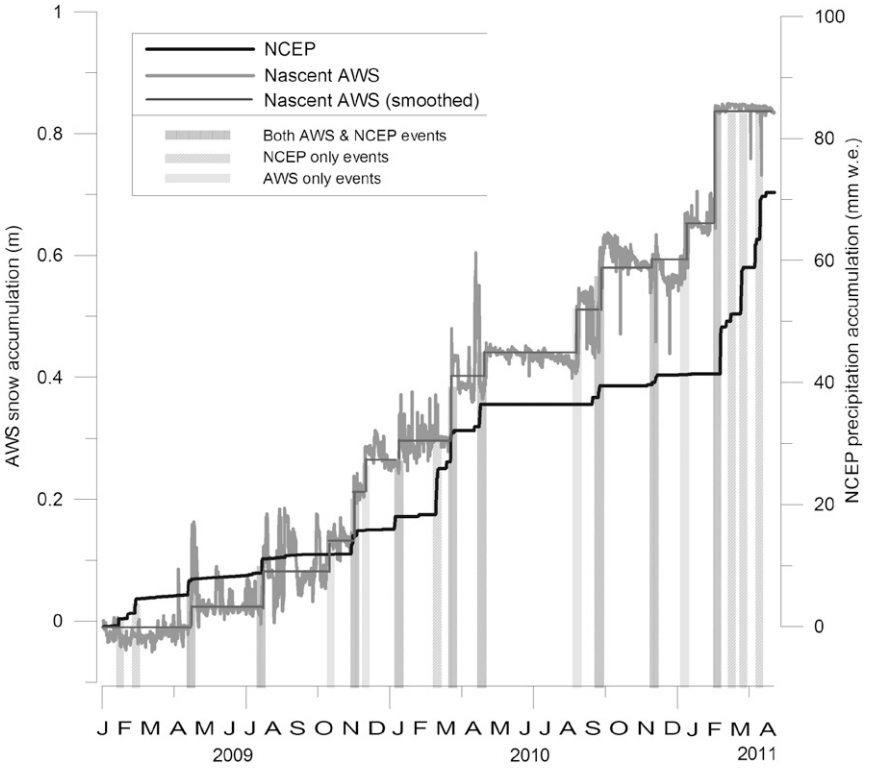

FIG. 4. Comparison of accumulated precipitation for the Nascent AWS (AMRC, SSEC, UW-Madison) with NCEP reanalysis (77.139°S, 178.125°W) for January 2009–April 2011. Reanalysis precipitation (black line) is in mm water equivalent; AWS precipitation (gray lines) is in meters of snow. The dark gray line overlaying the Nascent AWS measurements has been smoothed to show the large precipitation events only. Vertical bands indicate times when both datasets record large events, AWS-only events, and reanalysis-only events.

coastline. The types L and L-BA would be expected to drive moisture-depleted air masses that had traveled over the West Antarctic Ice Sheet to the site. The distinct differences in precipitation delivery shown here are similar to those found by Nicolas and Bromwich (2011) using the Antarctic Mesoscale Prediction System (AMPS) archive dataset.

Further breakdown of the precipitation by the relative size of precipitation event is also shown in Fig. 5. Three groups were chosen based on the overall distribution of the precipitation dataset. Very small and zero precipitation rates [less than 0.05 mm w.e. $(12\ h)^{-1}$] occurring 96.6% of the time account for less than 10% of the precipitation at the site. Of the remaining nonzero precipitation events, small events [less than 0.5 mm w.e. $(12\ h)^{-1}$] account for 38% of the total precipitation and large events [greater than 0.5 mm w.e. $(12\ h)^{-1}$] account for 53% of the total precipitation. The type L-R, which dominates as a precipitation source region, brings the majority of its snowfall in large amounts. The types L-A and Z also contribute significant percentages as large pulses of precipitation. For the type L-BA, precipitation is distributed primarily in small events, with the total amount reflecting the fact that this type is the most frequently occurring.

Because the Z type does not appear to be able to transport moist midlatitude air to the site, it is surprising to see this type associated with a large amount of precipitation. To consider why this might be so, the Z type was further divided into three subtypes with distinct synoptic differences (Fig. 6). The subtypes were derived by reclustering the Z type using the same clustering methodology as for the primary clustering. The Z subtypes are described as follows: Z zonal (Z_Z), zonal flow throughout the regions; Z low (Z_L), a low west of 180°; and Z trough (Z_T), a trough in the region. The frequency of these types as a percentage of the zonal type is shown on each map. While it can be seen that all three types are characterized by relatively weak gradients (as compared to the other main types), the type Z_L is distinguished by a low west of Roosevelt Island that could drive moist air south to the site and delivers 7.5% of the total precipitation (42% of the Z precipitation). The type Z_T, distinguished by a trough pattern and weak low just north of

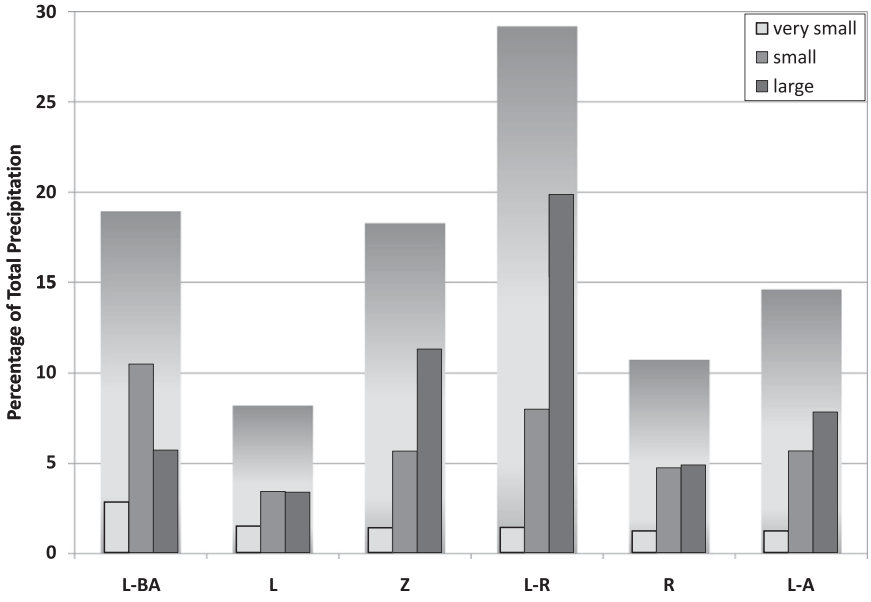

FIG. 5. Precipitation at Roosevelt Island with relation to the Ross Sea synoptic types for 1979–2011. Wide bars indicate percentage of total precipitation delivered to the Roosevelt Island site by each type (as in Fig. 2). Narrow bars indicate the composition of precipitation by size of event. Groupings are as follows: very small [$<$0.05 mm w.e. (12 h)$^{-1}$], small [0.05–0.5 mm w.e. (12 h)$^{-1}$], and large [$>$0.5 mm w.e. (12 h)$^{-1}$].

the site, delivers 4% of the total precipitation (23% of the Z precipitation). These two types indicate that weaker and/or more southerly positioned systems may play a significant role in precipitation in the Ross Sea region.

Total precipitation for the 32.5-yr period is 338 mm w.e., averaging ~10 mm w.e. yr^{-1} for the NCEP reanalysis data. From shallow firn cores and radar measurements across Roosevelt Island (Conway et al. 1999), actual annual precipitation is estimated to be on the order of 200 mm w.e. yr^{-1}. However, we do have some confidence in the qualitative ability (timing and relative amounts) of NCEP reanalysis to reconstruct precipitation on the Ross Ice Shelf from the Nascent AWS comparison. Two possible reasons the reanalysis may underestimate precipitation at Roosevelt Island are that 1) the summit of Roosevelt Island gets additional precipitation due to topographic uplift, being approximately 450 m above the surrounding ice shelf, and 2) mesoscale systems are not well captured by the reanalysis data because of its coarse resolution (Condron et al. 2006). Mesoscale systems are found in high densities in this region, particularly along the eastern Ross Ice Shelf, and have been shown to substantially contribute to precipitation along the Antarctic coast (e.g., Carrasco et al. 2003; Irving

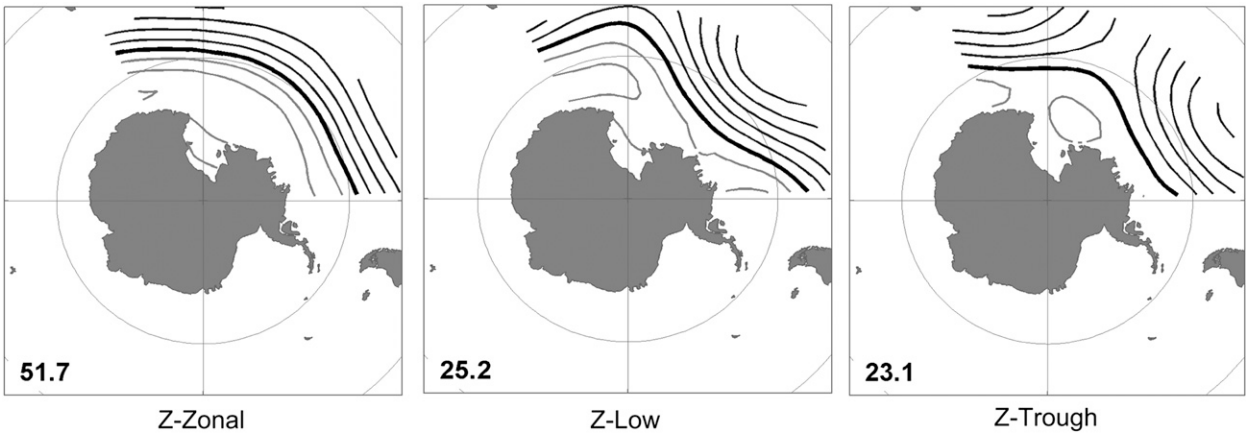

FIG. 6. Zonal subtypes (Z_Z, Z_L, and Z_T) and frequency of occurrence of each as percentage of the zonal type.

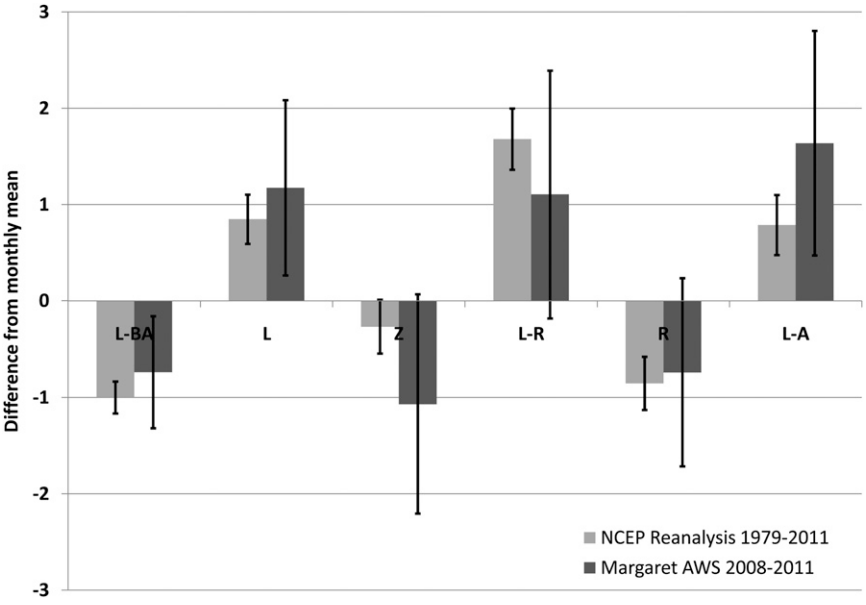

FIG. 7. Temperature departures from monthly means (with 95% confidence intervals indicated) at Roosevelt Island grouped by synoptic type (as in Fig. 2). Two temperature datasets are used: light gray bars are NCEP reanalysis from 1979 to 2011 and dark gray bars are for Margaret AWS (AMRC, SSEC, UW-Madison) from 13 Nov 2008 to 30 Jun 2011.

et al. 2010). The importance of these factors is of interest for interpreting Roosevelt Island climate data and is the subject of future and ongoing work.

f. Expression of synoptic types in temperature

The relationship between surface temperature at Roosevelt Island and synoptic types is shown in Fig. 7. The figure shows departures from monthly means and 95% confidence intervals for two temperature datasets: one is from a University of Wisconsin AWS located less than 100 km west of Roosevelt Island (Margaret AWS), and the other is NCEP reanalysis surface temperature for the grid box at 80°S, 160°W. The NCEP data are for the period January 1979–June 2011, and the AWS data are for 13 November 2008–30 June 2011. The reanalysis data shows significant temperature differences between synoptic types with average departures from monthly means varying between −1.0° and +1.7°C. Because the observed dataset is much shorter (~2.4 yr) than the reanalysis dataset (32.5 yr) the differences in temperature are not significant, but it is encouraging that the patterns and magnitudes are similar to those of the reanalysis data. As expected, the types L-R, and L-A bring warmer than average temperatures to the site as these types are associated with the relatively warm, moisture-bearing air from the Southern Ocean.

The type L shows warmer than average temperatures but brings the least amount of precipitation to the site, indicating that this type is associated with moisture-depleted but relatively warm air masses. The types L-BA and R are also low-precipitation types but are differentiated by lower than average temperatures, perhaps indicating these types are the primary drivers of the cold, dry drainage winds from the West Antarctic Ice Sheet (King and Turner 1997). The type Z also brings colder than average temperatures although over the longer dataset the average is close to zero (−0.3°C), indicating there may not be significant variability in temperature associated with this type.

4. Summary

This work provides the first synoptic-climatological classification of weather systems for Antarctica, focusing on the Ross Sea region and Antarctic coast across the Pacific sector. The six main synoptic types and three subtypes derived from NCEP reanalysis data describe the synoptic conditions for the period 1979–2011. The patterns describe realistic synoptic conditions for the region, representing the variability in the moisture-bearing low pressure systems that circulate around the Antarctic continent.

Seasonal variability of the synoptic types is in line with known patterns of variability such as the seasonal zonal shift of the ASL and pressure effects of ENSO and the SAM. The type L-R is negatively correlated with the

SOI and SAM while L-BA is positively correlated with the SOI and the SAM, indicating shifting of the position of the low farther east (west) toward (away from) the Antarctic Peninsula during La Niña (El Niño) and positive (negative) SAM conditions. Correlations of both types (L-BA and L-R) with the SAM are highest in the spring ($r = 0.75$ and $r = -0.55$ respectively) and nonexistent in the summer. Correlation of L-R with the SOI is also highest in the spring ($r = -0.61$).

Multiple linear regressions of the SOI and SAM indices improve on these correlations, indicating the reinforcing influence of these two climate cycles on the synoptic conditions of this region. The joint regressions show that the SOI and the SAM explain over 50% of the variability in L-BA and L-R in the spring and nearly 40% in autumn. Trends in the indices from 1979–2011 are also seen in trends of the occurrence of the synoptic types. Because the technique is shown to reflect variability in large-scale circulation in physically meaningful ways, we expect to see changes in the synoptic types (frequency or patterns) as the climate changes [e.g., as the positive SAM becomes more frequent (Marshall 2003)].

The synoptic types are also shown to reflect variability in measureable climate parameters such as precipitation and temperature, suggesting that this approach has some merit for studying surface climate at high latitudes. Using the Roosevelt Island ice core site as a case study, it is shown that the synoptic types bring very different amounts and size distributions of precipitation to Roosevelt Island. For example, the L-R synoptic type is shown to have a significant role in delivering precipitation to the site (~30% of total precipitation). That the frequency of L-R is strongly correlated with both the SOI and the SAM and exhibits a long-term trend suggests that an ice core record from Roosevelt Island may be able to offer significant insights into the long-term variability of these climate drivers.

There are many potential applications for using synoptic classification to help understand how local climate parameters relate to climate variability in Antarctica. Future work with the Ross Sea synoptic types will focus on investigating the relationship to meteorological parameters at other sites and relating the synoptic types to other climate parameters (e.g., sea ice and snow chemistry).

Acknowledgments. The authors greatly appreciate the support of the University of Wisconsin—Madison Automatic Weather Station Program and Antarctic Meteorological Research Center for the AWS datasets and Matthew Lazzara in particular for information provided on the Antarctic AWS datasets. We also appreciate use of NCEP reanalysis data provided by the NOAA/OAR/ESRL PSD, Boulder, Colorado. Two of the authors (SD and JR) were part funded through core funding from the New Zealand Ministry of Science and Innovation.

REFERENCES

Bromwich, D. H., 1988: Snowfall in high southern latitudes. *Rev. Geophys.,* **26,** 149–168.

——, and R. L. Fogt, 2004: Strong trends in the skill of the ERA-40 and NCEP–NCAR reanalyses in the high and midlatitudes of the Southern Hemisphere, 1958–2001. *J. Climate,* **17,** 4603–4619.

——, A. N. Rogers, P. Kållberg, R. I. Cullather, J. W. C. White, and K. J. Kreutz, 2000: ECMWF analyses and reanalyses depiction of ENSO signal in Antarctic precipitation. *J. Climate,* **13,** 1406–1420.

——, R. L. Fogt, K. I. Hodges, and J. E. Walsh, 2007: A tropospheric assessment of the ERA-40, NCEP, and JRA-25 global reanalyses in the polar regions. *J. Geophys. Res.,* **112,** D10111, doi:10.1029/2006JD007859.

——, J. P. Nicholas, and A. J. Monaghan, 2011: An assessment of precipitation changes over Antarctica and the Southern Ocean since 1989 in contemporary global reanalyses. *J. Climate,* **24,** 4189–4209.

Carrasco, J. F., D. H. Bromwich, and A. J. Monaghan, 2003: Distribution and characteristics of mesoscale cyclones in the Antarctic: Ross Sea eastward to the Weddell Sea. *Mon. Wea. Rev.,* **131,** 289–301.

Condron, A., G. R. Bigg, and I. A. Renfrew, 2006: Polar mesoscale cyclones in the northeast Atlantic: Comparing climatologies from ERA-40 and satellite imagery. *Mon. Wea. Rev.,* **134,** 1518–1533.

Conway, H., B. L. Hall, G. H. Denton, A. M. Gades, and E. D. Waddington, 1999: Past and future grounding-line retreat of the West Antarctic Ice Sheet. *Science,* **286,** 280–283.

Cullather, R. I., D. H. Bromwich, and M. L. Van Woert, 1996: Interannual variations in Antarctic precipitation related to El Niño-Southern Oscillation. *J. Geophys. Res.,* **101,** 19 109–19 118.

——, ——, and ——, 1998: Spatial and temporal variability of Antarctic precipitation from atmospheric methods. *J. Climate,* **11,** 334–367.

Fogt, R. L., and D. H. Bromwich, 2006: Decadal variability of the ENSO teleconnection to the high-latitude South Pacific governed by coupling with the southern annular mode. *J. Climate,* **19,** 979–997.

——, ——, and K. M. Hines, 2011: Understanding the SAM influence on the South Pacific ENSO teleconnection. *Climate Dyn.,* **36,** 1555–1576.

——, A. J. Wovrosh, R. A. Langen, and I. Simmonds, 2012: The characteristic variability and connection to the underlying synoptic activity of the Amundsen-Bellingshausen Seas low. *J. Geophys. Res.,* **117,** D07111, doi:10.1029/2011JD017337.

Gregory, S., and D. Noone, 2008: Variability in the teleconnection between the El Niño–Southern Oscillation and West Antarctic climate deduced from West Antarctic ice core isotope records. *J. Geophys. Res.,* **113,** D17110, doi:10.1029/2007JD009107.

Helsen, M. M., R. S. W. van de Wal, and M. R. Van den Broeke, 2007: The isotopic composition of present-day Antarctic snow in a Lagrangian atmospheric simulation. *J. Climate,* **20,** 739–756.

Irving, D., I. Simmonds, and K. Keay, 2010: Mesoscale cyclone activity over the ice-free Southern Ocean: 1999–2008. *J. Climate,* **23,** 5404–5420.

Kalnay, E., and Coauthors, 1996: The NCEP/NCAR 40-Year Reanalysis Project. *Bull. Amer. Meteor. Soc.,* **77,** 437–470.

Kidson, J. W., 1994: An automated procedure for the identification of synoptic types applied to the New Zealand region. *Int. J. Climatol.,* **14,** 711–721.

——, 1999: Principal modes of Southern Hemisphere low frequency variability obtained from NCEP/NCAR reanalyses. *J. Climate,* **12,** 2808–2830.

——, 2000: An analysis of New Zealand synoptic types and their use in defining weather regimes. *Int. J. Climatol.,* **20,** 299–316.

——, and J. A. Renwick, 2002: The Southern Hemisphere evolution of ENSO during 1981–99. *J. Climate,* **15,** 847–863.

King, J. C., and J. Turner, 1997: *Antarctic Meteorology and Climatology.* Cambridge University Press, 409 pp.

Knuth, S. L., G. J. Tripoli, J. E. Thom, and G. A. Weidner, 2010: The influence of blowing snow and precipitation on snow depth change across the Ross Ice Shelf and Ross Sea regions of Antarctica. *J. Appl. Meteor. Climatol.,* **49,** 1306–1321.

Krinner, G., O. Magand, I. Simmonds, C. Genthon, and J. L. Dufresne, 2007: Simulated Antarctic precipitation and surface mass balance at the end of the twentieth and twenty-first centuries. *Climate Dyn.,* **28,** 215–230.

Kwok, R., and J. C. Comiso, 2002: Spatial patterns of variability in Antarctic surface temperature: Connections to the Southern Hemisphere annular mode and the Southern Oscillation. *Geophys. Res. Lett.,* **29,** 1705, doi:10.1029/2002GL015415.

L'Heureux, M. L., and D. W. J. Thompson, 2006: Observed relationships between the El Niño–Southern Oscillation and the extratropical zonal-mean circulation. *J. Climate,* **19,** 276–287.

Lorrey, A., A. M. Fowler, and J. Salinger, 2007: Regional climate regime classification as a qualitative tool for interpreting multi-proxy palaeoclimate data spatial patterns: A New Zealand case study. *Palaeogeogr. Palaeoclimatol. Palaeoecol.,* **253,** 407–433.

MacQueen, J., 1967: Some methods for classification and analysis of multivariate observations. *Proc. Fifth Berkeley Symp. on Mathematics and Statistical Probability,* Berkeley, CA, University of California, Berkeley, 281–297.

Markle, B. R., N. A. N. Bertler, K. E. Sinclair and S. B. Sneed, 2012: Synoptic variability in the Ross Sea region, Antarctica, as seen from back-trajectory modeling and ice core analysis. *J. Geophys. Res.,* **117,** D02113, doi:10.1029/2011JD016437.

Marshall, G. J., 2003: Trends in the southern annular mode from observations and reanalyses. *J. Climate,* **16,** 4134–4143.

Mayewski, P. A., and Coauthors, 2005: The International Trans-Antarctic Scientific Expedition (ITASE): An overview. *Ann. Glaciol.,* **41,** 180–185.

Mellor, M., Ed., 1964: *Antarctic Snow and Ice Studies.* Antarctic Research Series, Vol. 2, Amer. Geophys. Union, 286 pp.

Nicolas, J. P., and D. H. Bromwich, 2011: Climate of West Antarctica and influence of marine air intrusions. *J. Climate,* **24,** 49–67.

Noone, D., and I. Simmonds, 2002: Annular variations in moisture transport mechanisms and the abundance of $\delta^{18}O$ in Antarctic snow. *J. Geophys. Res.,* **107,** 4742, doi:10.1029/2002JD002262.

——, J. Turner, and R. Mulvaney, 1999: Atmospheric signals and characteristics of accumulation in Dronning Maud Land, Antarctica. *J. Geophys. Res.,* **104** (D16), 19 191–19 211.

O'Donnell, R., N. Lewis, S. McIntyre and J. Condon, 2011: Improved methods for PCA-based reconstructions: Case study using the Steig et al. (2009) Antarctic temperature reconstruction. *J. Climate,* **24,** 2099–2115.

Pezza, A. B., H. A. Rashid, and I. Simmonds, 2012: Climate links and recent extremes in Antarctic sea ice, high-latitude cyclones, southern annular mode and ENSO. *Climate Dyn.,* **38,** 57–73.

Purdie, H., A. Mackintosh, W. Lawson, and B. Anderson, 2011: Synoptic influences on snow accumulation on glaciers east and west of a topographic divide: Southern Alps, New Zealand. *Arct. Antarct. Alp. Res.,* **43,** 82–94.

Renwick, J. A., 2002: Southern Hemisphere circulation and relations with sea ice and sea surface temperature. *J. Climate,* **15,** 3058–3068.

——, 2011: Kidson's synoptic weather types and surface climate variability over New Zealand. *Wea. Climate,* **31,** 2–23.

——, R. J. Hurst, and J. W. Kidson, 1998: Climatic influences on the survival of southern Gemfish (*Rexea Solandri, Gempylidae*) in New Zealand waters. *Int. J. Climatol.,* **18,** 1655–1667.

Rignot, E., J. L. Bamber, M. R. van den Broeke, C. Davis, Y. H. Li, W. J. van de Berg, and E. van Meijgaard, 2008: Recent Antarctic ice mass loss from radar interferometry and regional climate modeling. *Nat. Geosci.,* **1,** 106–110.

Schneider, D. P., E. J. Steig, and J. C. Comiso, 2004: Recent climate variability in Antarctica from satellite-derived temperature data. *J. Climate,* **17,** 1569–1583.

Sheridan, S. C., and C. C. Lee, 2010: Synoptic climatology and the general circulation model. *Prog. Phys. Geogr.,* **34,** 101–109.

Simmonds, I., 2003: Modes of atmospheric variability over the Southern Ocean. *J. Geophys. Res.,* **108,** 8078, doi:10.1029/2000JC000542.

——, and D. A. Jones, 1998: The mean structure and temporal variability of the semiannual oscillation in the southern extratropics. *Int. J. Climatol.,* **18,** 473–504.

——, and K. Keay, 2000: Variability of Southern Hemisphere extratropical cyclone behavior, 1958–97. *J. Climate,* **13,** 550–561.

——, ——, and E. Lim, 2003: Synoptic activity in the seas around Antarctica. *Mon. Wea. Rev.,* **131,** 272–287.

Sinclair, K. E., N. A. N. Bertler, and W. J. Trompetter, 2010: Synoptic controls on precipitation pathways and snow delivery to high-accumulation ice core sites in the Ross Sea region, Antarctica. *J. Geophys. Res.,* **115,** D22112, doi:10.1029/2010JD014383.

Smithson, P. A., 1986: Synoptic and dynamic climatology. *Prog. Phys. Geogr.,* **10,** 100–110.

Stammerjohn, S. E., D. G. Martinson, R. C. Smith, X. Yuan, and D. Rind, 2008: Trends in Antarctic annual sea ice retreat and advance and their relation to El Niño–Southern Oscillation and southern annular mode variability. *J. Geophys. Res.,* **113,** C03S90, doi:10.1029/2007JC004269.

Thomas, E. R., and T. J Bracegirdle, 2009: Improving ice core interpretation using in situ and reanalysis data. *J. Geophys. Res.,* **114,** D20116, doi:10.1029/2009JD012263.

Thompson, D. W. J., and J. M. Wallace, 2000: Annular modes in the extratropical circulation. Part I: Month-to-month variability. *J. Climate,* **13,** 1000–1016.

Trenberth, K. E., 1997: The definition of El Niño. *Bull. Amer. Meteor. Soc.,* **78,** 2771–2777.

Turner, J., 2004: The El Niño-Southern Oscillation and Antarctica. *Int. J. Climatol.,* **24,** 1–31.

——, and Coauthors, 2005a: Antarctic climate change during the last 50 years. *Int. J. Climatol.,* **25,** 279–294.

——, T. Lachlan-Cope, S. Colwell, and G. J. Marshall, 2005b: A positive trend in western Antarctic Peninsula precipitation over the last 50 years reflecting regional and

Antarctic-wide atmospheric circulation changes. *Ann. Glaciol.,* **41,** 85–91.

van den Broeke, M. R., 1998: The semi-annual oscillation and Antarctic climate. Part 1: Influence on near surface temperatures (1957-1979). *Antarct. Sci.,* **10,** 175–183.

——, 2000: On the interpretation of Antarctic temperature trends. *J. Climate,* **13,** 3885–3889.

van Loon, H., 1967: The half-yearly oscillations in the middle and high southern latitudes and the coreless winter. *J. Atmos. Sci.,* **24,** 472–486.

Yarnal, B., 1993: *Synoptic Climatology in Environmental Analysis.* Bellhaven Press, 195 pp.

——, A. C. Comrie, B. Frakes, and D. P. Brown, 2001: Developments and prospects in synoptic climatology. *Int. J. Climatol.,* **21,** 1923–1950.

Zou, C. Z., M. L. Van Woert, C. Y. Xu, and K. Syed, 2004: Assessment of the NCEP–DOE Reanalysis-2 and TOVS Pathfinder A moisture fields and their use in Antarctic net precipitation estimates. *Mon. Wea. Rev.,* **132,** 2463–2476.